Continental Growth and Thermal Convection in the Earth's Mantle

Uwe Walzer[1], Roland Hendel[1], and John Baumgardner[2]

[1] Institut für Geowissenschaften, Friedrich-Schiller-Universität, Burgweg 11, 07749 Jena, Germany u.walzer@uni-jena.de
[2] Dept. Earth Planet. Science, University of California, Berkeley, CA 94720, USA

Summary. The main subject of this paper is the numerical simulation of the chemical differentiation of the Earth's mantle. This differentiation induces the generation and growth of the continents and, as a complement, the formation and augmentation of the depleted MORB mantle. Here, we present for the first time a solution of this problem by an integrated theory in common with the problem of thermal convection *in a 3-D compressible spherical-shell mantle*. The whole coupled thermal and chemical evolution of mantle plus crust was calculated starting with the formation of the *solid-state* primordial silicate mantle. No restricting assumptions have been made regarding number, size and form of the continents. It was, however, implemented that moving oceanic plateaus touching a continent are to be accreted to this continent at the corresponding place. The model contains a mantle-viscosity profile with a usual asthenosphere beneath a lithosphere, a highly viscous transition zone and a second low-viscosity layer below the 660-km mineral phase boundary. The central part of the lower mantle is highly viscous. This explains the fact that there are, regarding the incompatible elements, chemically different mantle reservoirs in spite of perpetual stirring during more than 4.49×10^9 a. The highly viscous central part of the lower mantle also explains the relatively slow lateral movements of CMB-based plumes, slow in comparison with the lateral movements of the lithospheric plates. The temperature- and pressure-dependent viscosity of the model is complemented by a viscoplastic yield stress, σ_y. The paper includes a comprehensive variation of parameters, especially the variation of the viscosity-level parameter, r_n, the yield stress, σ_y, and the temporal average of the Rayleigh number. In the r_n-σ_y plot, a central area shows runs with realistic distributions and sizes of continents. This area is partly overlapping with the r_n-σ_y areas of piecewise plate-like movements of the lithosphere and of realistic values of the surface heat flow and Urey number. Numerical problems are discussed in Section 3.

1 Introduction

Investigations of the isotopic compositions of SNC meteorites and lunar rocks show a relatively quick chemical differentiation of Mars and Moon within the

first 200 Ma (Norman et al., 2003; Nyquist et al., 2001). It is probable that not only the iron cores of these planetary bodies were formed rather quickly but also an early silicate crust developed from a magma ocean. A similar mechanism can be expected for the early Earth. In the case of the Earth, however, there are three additional modes of growth of the total continental mass (Hofmann, 2004) which continue to add juvenile mass in batches distributed over the whole geological history. The continental crust (CC) grows episodically (Condie, 2003). U, Th, K and other incompatible elements will be enriched in CC leaving behind parts of the mantle depleted in these elements: This reservoir of the mantle is called depleted MORB mantle (DMM) where MORB stands for mid-oceanic ridge basalt. These processes are in fact much more complex (Porcelli and Ballentine, 2002; Hofmann, 2004; Bennett, 2004; Rudnick and Gao, 2004; Fitton et al., 2004; Stracke et al., 2005; Walzer et al., 2006). Furthermore, there is still some doubt as to whether the rich part of the mantle below DMM is quasi-primordial or processed or mainly processed and to a lower degree quasi-primordial. Rich means rich in incompatible elements. It is only clear that this non-DMM part of the mantle must be richer in U,

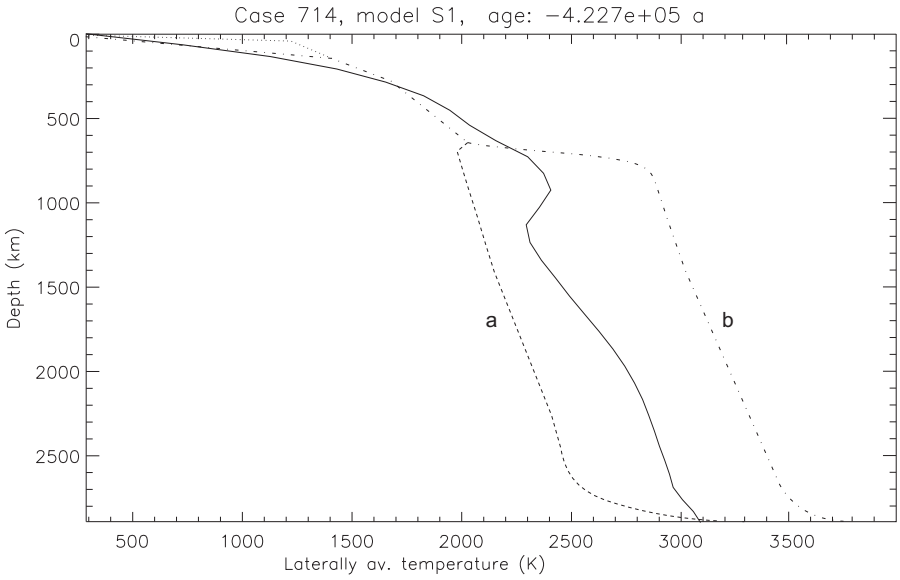

Fig. 1. The solid curve represents the laterally averaged temperature of the geological present time for a reference run with a viscoplastic yield stress of $\sigma_y = 135$ MPa and a viscosity-level parameter $r_n = -0.6$. Cf. Eqs. (1) and (2). The CMB temperature, T_c, is laterally constant but variable in time according to the parameterized heat balance of the Earth's core. The range of possible mantle geotherms according to parameterized models given by Schubert et al. (2001) is shown for comparison. Label a and b denote geotherms of whole-mantle and partially layered convection, respectively. The dotted line stands for a mid-oceanic ridge geotherm.

Th and K, richer than DMM. Otherwise the requirements of energy supply would not be fulfilled.

The lateral movements of lithospheric plates, the collisions of continents, the collisions of continents and oceanic plates as well as orogenesis are caused by thermal solid-state convection of the mantle (Schubert et al., 2001). The energy sources of this convective motor are the kinetic energy of the Earth's accretion, the potential energy of the gravitational differentiation of a possibly homogeneous primordial Earth into an iron core and a silicate primordial mantle, and the nuclear bonding energy that is released by the decay of the radionuclides ^{238}U, ^{235}U, ^{232}Th and ^{40}K. Minor energy sources are the heat of tidal friction and the latent heat due to the growth of the inner core at the expense of the outer core. This heat is released by the cooling of the Earth.

2 Theory

We solve the balance equations of mass, momentum and energy using the anelastic liquid approximation in the formulation given by Walzer et al. (2003b). Furthermore, the balance equations of the mentioned radionuclides plus their corresponding daughter nuclides are taken into account. We supple-

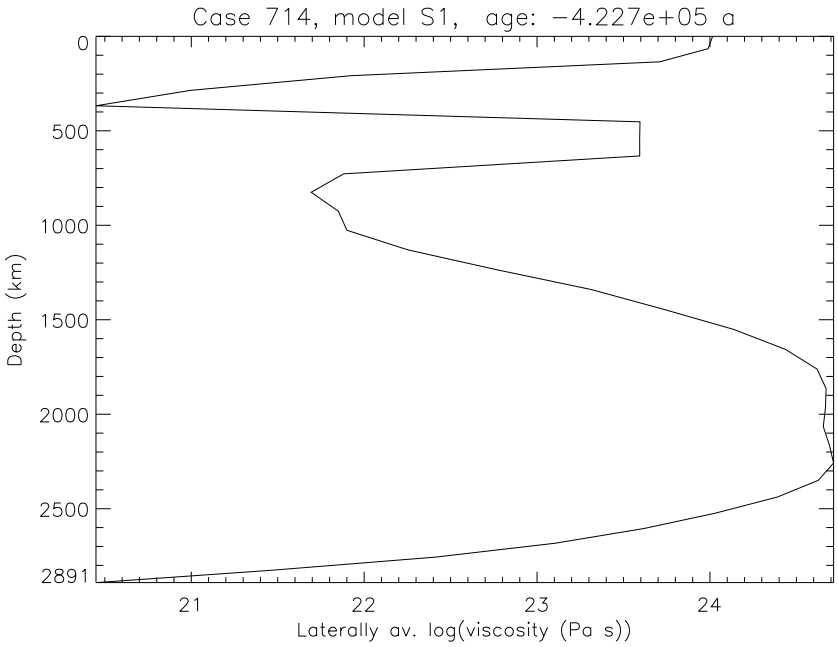

Fig. 2. The laterally averaged shear viscosity of the reference run for the geological present time.

ment the viscous constitutive equation by a viscoplastic yield stress, σ_y, for the uppermost 285 km and by a special viscosity profile for the initial temperature. This viscosity profile has been derived by Walzer et al. (2004a). In the present paper, the equations of chemical differentiation of oceanic plateaus plus the above mentioned equations are simultaneously solved. The new features of the theory are given in Walzer et al. (2006).

Here are only some remarks on the viscosity law. The shear viscosity, η, is calculated by

$$\eta(r,\theta,\phi,t) = 10^{r_n} \cdot \frac{\exp(c\,\overline{T_m/T_{av}})}{\exp(c\,\overline{T_m/T_{st}})} \cdot \eta_3(r) \cdot \exp\left[c_t \cdot T_m \left(\frac{1}{T} - \frac{1}{T_{av}}\right)\right] \quad (1)$$

where r is the radius, θ the colatitude, ϕ the longitude, t the time, r_n the viscosity-level parameter, T_m the melting temperature, T_{av} the laterally averaged temperature, T_{st} the initial temperature profile, T the temperature as a function of r, θ, ϕ, t. The quantity $\eta_3(r)$ is the viscosity profile at the initial temperature and for $r_n = 0$. So, $\eta_3(r)$ describes the dependence of the viscosity on pressure and on the mineral phase boundaries. The second factor of the right-hand side of Eq. (1) describes the increase of the viscosity profile with the cooling of the Earth. For $MgSiO_3$ perovskite we should insert c=14, for MgO wüstite c=10 according to Yamazaki and Karato (2001). So, the lower-mantle c should be somewhere between these two values. For numerical reasons, we are able to use only c=7. In the lateral-variability term, we inserted $c_t = 1$. For the uppermost 285 km of the mantle (plus crust), an effective viscosity, η_{eff}, was implemented where

$$\eta_{eff} = \min\left[\eta(P,T), \frac{\sigma_y}{2\dot{\varepsilon}}\right] \quad (2)$$

The pressure is denoted by P, the second invariant of the strain-rate tensor by $\dot{\varepsilon}$.

Oceanic plateaus are driven on the surface of the moving oceanic lithosphere near to the continents like on a conveyor belt. They will be subducted to a depth of about 100 km and suffer a further chemical differentiation. The emerging andesitic magmas will be added to the continent. So, the total mass of the continents increases generating a growing DMM or MORB source reservoir of the mantle, that is depleted in incompatible elements, as a countermove. The present numerical model depends only slightly on the question whether, except DMM, only FOZO, HIMU, EM1 and EM2 exist in the mantle (see Hofmann, 2004; Stracke et al., 2005) or whether there are additionally nearly primordial parts of the mantle (Bennett, 2004).

Although mantle convection is working by solid-state creeping, we calculate the process using the differential equations of a compressible anelastic liquid that is heated from within by the decay of ^{238}U, ^{235}U, ^{232}Th and ^{40}K. The mantle is additionally slightly heated from the core-mantle boundary (CMB). For this purpose, we use a parameterized cooling-core model.

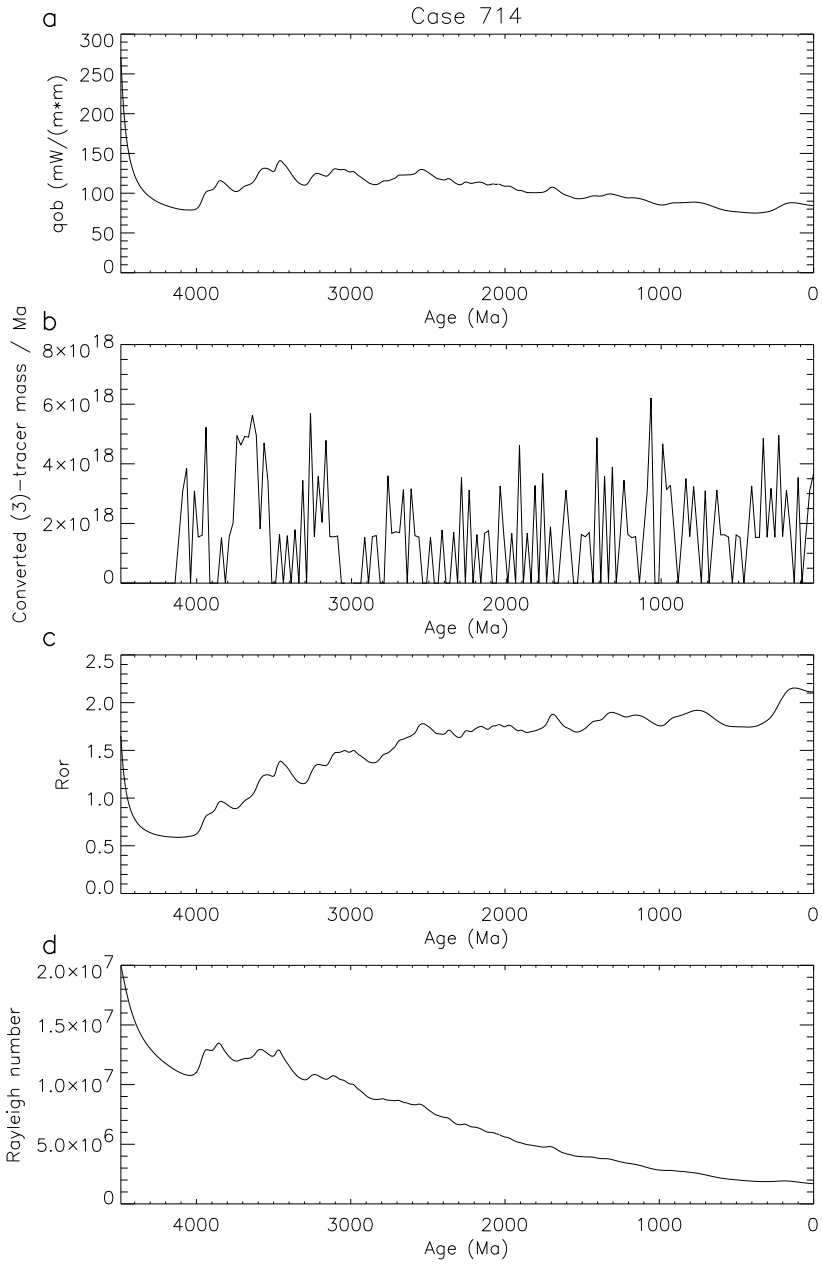

Fig. 3. (a) The evolution of the laterally averaged surface heat flow, *qob*. **(b)** Juvenile contributions to the total mass of the continents, expressed as converted (3)-tracer mass per Ma, as a function of time. **(c)** The evolution of the reciprocal value of the Urey number. *Ror* means *r*atio of the surface heat *o*utflow per unit time to the mantle's *r*adiogenic heat production per unit time. **(d)** The evolution of the Rayleigh number.

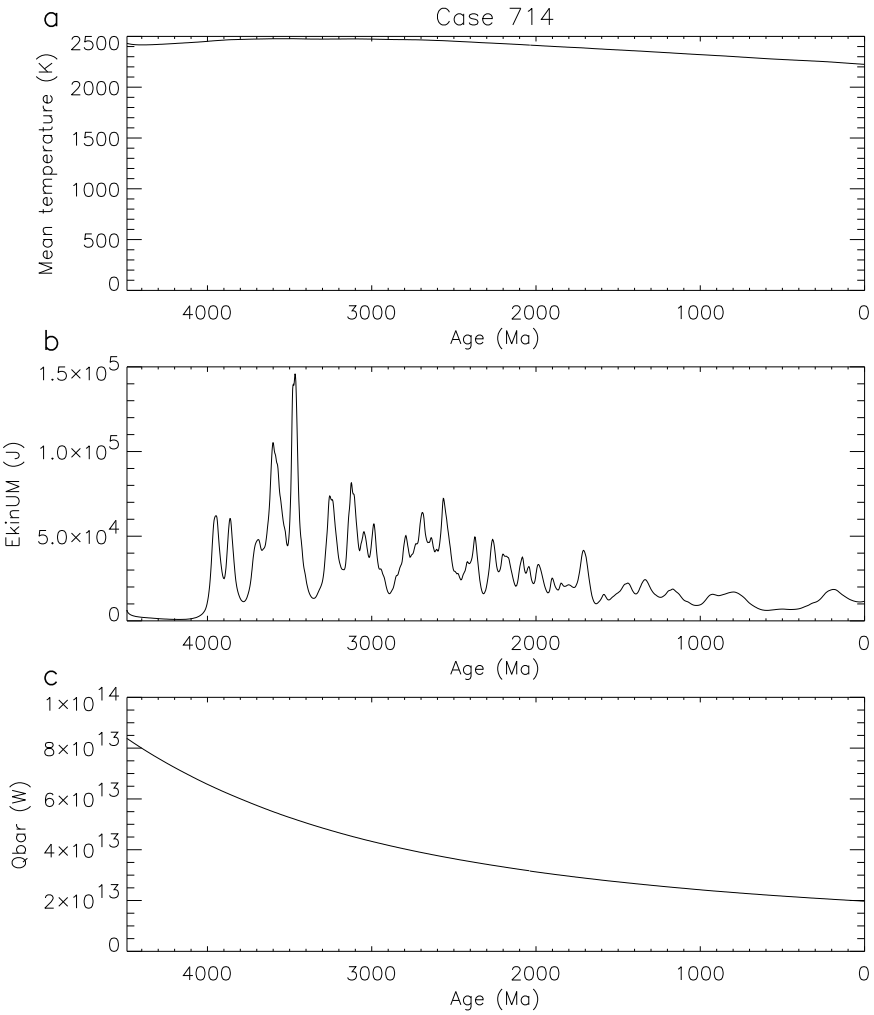

Fig. 4. (a) The evolution of the volume-averaged mean temperature of the mantle. **(b)** The kinetic energy of the thermal convection in the upper mantle, *EkinUM*, as a function of time. **(c)** The evolution of the power of the internal radiogenic heat generation of the mantle, *Qbar*.

The CMB temperature, T_c, is laterally constant at a particular time. But T_c decreases as a function of time.

There is an open principal question: Why can we, at present, observe reservoirs with different abundances of the mentioned radionuclides in the interior of the mantle in spite of the continual stirring due to convection enduring for more than 4.49×10^9 a of the existence of the solid-state silicate

mantle? A mathematical description of the segregation mechanism is given by Walzer et al. (2006).

3 Numerical aspects

The total pressure dependence and the radial temperature dependence of viscosity is completely taken into account. For numerical reasons, however, only a part of the lateral temperature dependence of the viscosity could be used. At the mineral phase boundaries in the interior of the Earth's mantle, there are not only discontinuities of the seismic velocities and of the density but also jumps of activation volumes, activation energies and, therefore, of activation enthalpies. Since the viscosity depends exponentially on the activation enthalpy of the prevailing creeping process, the conclusion is inescapable that there are considerable viscosity jumps at the upper and lower surfaces of the transition zone. These jumps cause numerical problems in the solution of the balance equations. The problems have been solved. Nevertheless, our group

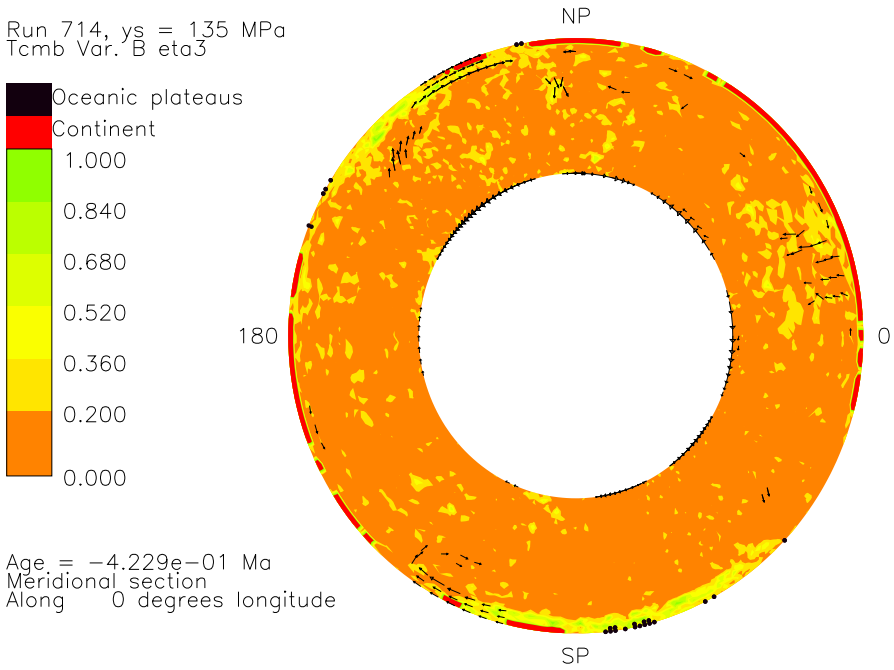

Fig. 5. The result of the chemical evolution of the silicate spherical shell of the Earth for the geological present time. Strongly depleted parts of the mantle are denoted by yellow or greenish areas. Less depleted and rich parts of the mantle have orange colors. Depleted means with a low content of incompatible elements like U,Th,K etc. Continents are depicted in red. Black dots represent oceanic plateaus.

is searching for more effective solutions of the numerical jump problem. The minor discontinuity at a depth of 520 km has been neglected.

The mantle has been treated as a thick spherical shell. The discretization is made by projection of the edges of a concentric regular icosahedron (situated in the core) onto spherical shell surfaces with different radial distances from the center. These surfaces subdivide the mantle into thin shells. A first step of grid refinement is the bipartition of the edges of the spherical triangles into equal parts. Connecting the new points by great circles, we obtain four smaller triangles from each starting triangle. The refinement can be augmented by succesive steps of this kind. We can use different formulae for the distribution of the radial distances of the spherical grid surfaces. In this paper, we used exclusively a grid with isometric grid cells, as good as possible. The grid is non-adaptive. The Navier-Stokes equations as well as pressure and creeping velocity are discretized by finite elements. Piecewise

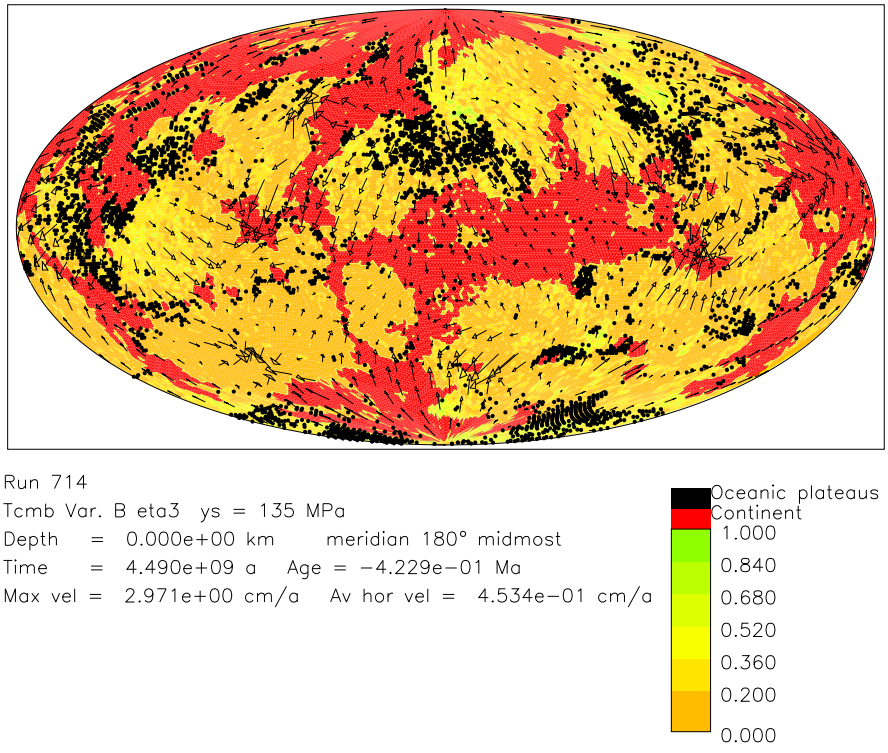

Fig. 6. The distribution of the red continents and the black oceanic plateaus at the Earth's surface for the geological present time of a reference run with a yield stress $\sigma_y = 135$ MPa and a viscosity-level parameter $r_n = -0.6$. Their are no prescriptions regarding number, size or form of continents in this model S3. Arrows represent the creeping velocities. The oceanic lithosphere is shown in yellowish colors.

linear basis functions have been applied for the creeping velocity, piecewise constant or also piecewise linear basis functions are used for the pressure. The equations for pressure and creeping velocity have been simultaneously solved by the Ramage-Wathen procedure. This is an Uzawa algorithm. The energy equation has been solved using an iterative multidimensional positive-definite advection-transport algorithm with explicit time steps (Bunge and Baumgardner, 1995). In the Ramage-Wathen procedure, the corresponding equation systems are solved by a multigrid procedure and a Jacobi smoother. In the multigrid procedure, prolongation and restriction are matrix-dependently executed. Only in this way, it was possible to handle the strong variations and jumps of the coefficients that mimic the strong viscosity gradients (Yang, 1997). Radial and horizontal lines are used in the Jacobi smoother. For the formulation of chemical differentiation, we used a tracer modul developed by Dave Stegman. This modul contains a second-order Runge-Kutta procedure to move the tracers in the creeping-velocity field. Each tracer conveys, e.g., the abundances of the radionuclides. In this case, it is an active tracer since

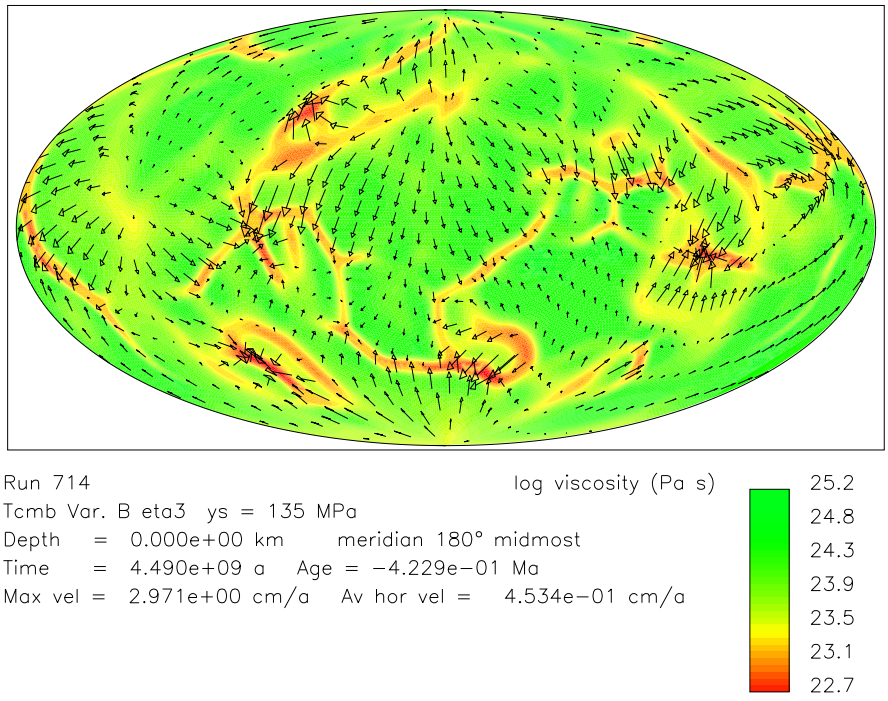

Fig. 7. Equal-area projection with the surface distribution of log viscosity (Pa·s) for the geological present time (colors) for $\sigma_y = 135$ MPa and $r_n = -0.6$. The creeping velocities (arrows) show a plate-like distribution. Elongated high strain rate zones have reduced viscosity due to viscoplastic yielding.

the multitude of tracers determines the heat production rate per unit volume dependent on time and location vector.

The FORTRAN code is parallelized by domain decomposition and explicit message passing (MPI)(Bunge, 1996).

4 The developing stages of the present thermal and chemical evolution model of the Earth's mantle

Our latest papers, [25], [26], second part of [27], [28], [29], use a viscosity profile of the mantle that is derived from the seismic model PREM (Dziewonski and Anderson, 1981) and solid-state physics. The latter term denotes not only theoretical-physics papers but also the experimental results of the Karato group. Meanwhile, the steep viscosity gradients at the upper and lower surface of the transition zone could be handled. Formerly [24], it was necessary

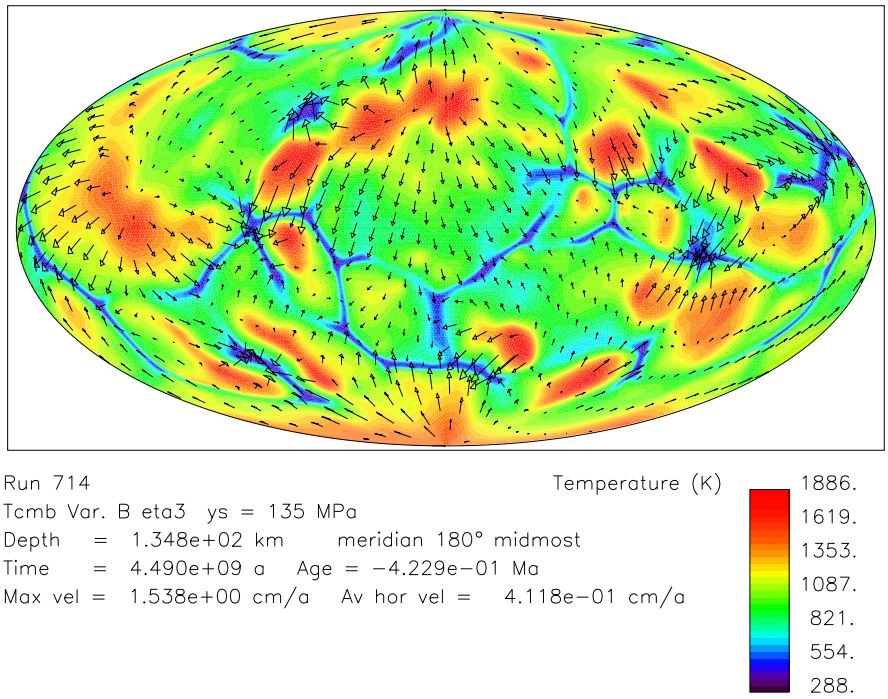

Fig. 8. Temperature distribution (colors) and creeping velocities (arrows) for a reference run with $\sigma_y = 135$ MPa and $r_n = -0.6$, for the geological present. The shown area is an equal-area projection of a spherical surface in 134.8 km of depth. The narrow blue subducting zones can be found also in deeper equal-area projections of temperature distribution. The slab-like features are rather narrow in comparison with the broad upwelling zones.

to slope the viscosity jumps stronger. In [24], a constant CMB heat flow of 28.9 mW/m^2 was assumed using Anderson (1998). Regarding the constancy with respect to time, this assumption was founded on Stevenson et al. (1983), Stacey (1992) and Schubert et al. (2001). In [25], [26], second part of [27], [28], [29], however, it is assumed that the CMB is *laterally* isothermal. A core-cooling model was implemented: the CMB temperature was determined after each time step, in dependence from the computed CMB heat flow (Steinbach et al., 1993; Honda and Iwase, 1996). Now, both, CMB temperature and CMB heat flow, are dependent on time. As a third innovation, the Newtonian rheology has been supplemented by a *viscoplastic yield stress,* σ_y. We made a variation of the parameters and found *stable plate-like solutions on a sphere* for a central σ_y-$Ra(2)$ region where $Ra(2)$ is the temporal average of the Rayleigh number, averaged over the last 2000 Ma [25], [26]. This model, S2, had, however, only oceanic lithospheric plates but no continents. We used exclusively models of whole-mantle convection with two interior phase boundaries and si-

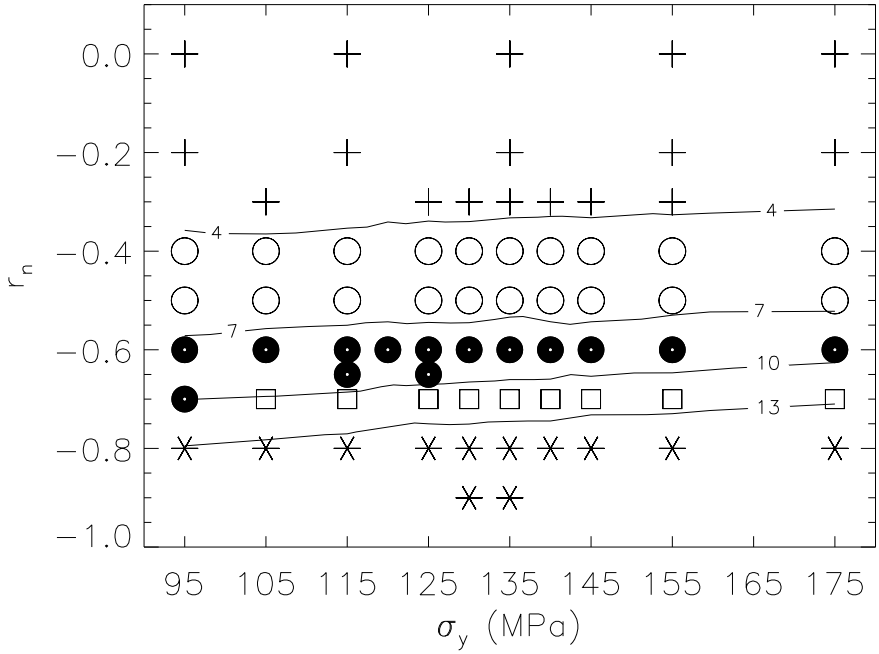

Fig. 9. The time average of the Rayleigh number, Ra, as a function of yield stress, σ_y, and viscosity-level parameter, r_n. Each sign represents one run. Asterisks stand for runs with $13 \times 10^6 \leq Ra$. White squares represent runs with $10 \times 10^6 \leq Ra < 13 \times 10^6$. Little black disks with a white center typify runs with $7 \times 10^6 \leq Ra < 10 \times 10^6$. White circles denote runs with $4 \times 10^6 \leq Ra < 7 \times 10^6$. Finally, plus signs stand for runs with $Ra < 4 \times 10^6$.

multaneously the long-term thermal evolution from the very beginning of the existence of the solid silicate mantle. The modelled mantle was compressible with variable viscosity and time-dependent heating from within plus a slight heating from below. The dynamical results using our own mantle viscosity profile have been compared with our dynamical results using viscosity profiles of Kaufmann and Lambeck (2002) and King and Masters (1992) [26].

In [24], another viscosity profile with two low-viscosity layers and a *purely viscous* constitutive equation is applied. This assumptions lead to reticularly connected very thin plate-like downwellings that dip perpendicularly into the mantle. It is no surprise that there are neither plates at the surface nor transform faults. If $Nu_{(2)}$ stands for the temporal average of the Nusselt number, averaged over the last 2000 Ma, and $Ra_{(2)}$ is the corresponding mean for the Rayleigh number then we find $Nu_{(2)} = 0.120 Ra_{(2)}^{0.295}$ for a wide parameter range.

In [28] that is based on [25] and [26], the growing values of the viscosity profile due to cooling of the Earth are taken into account. Therefore, the laterally averaged surface heat flow as a function of time, the Urey and Rayleigh

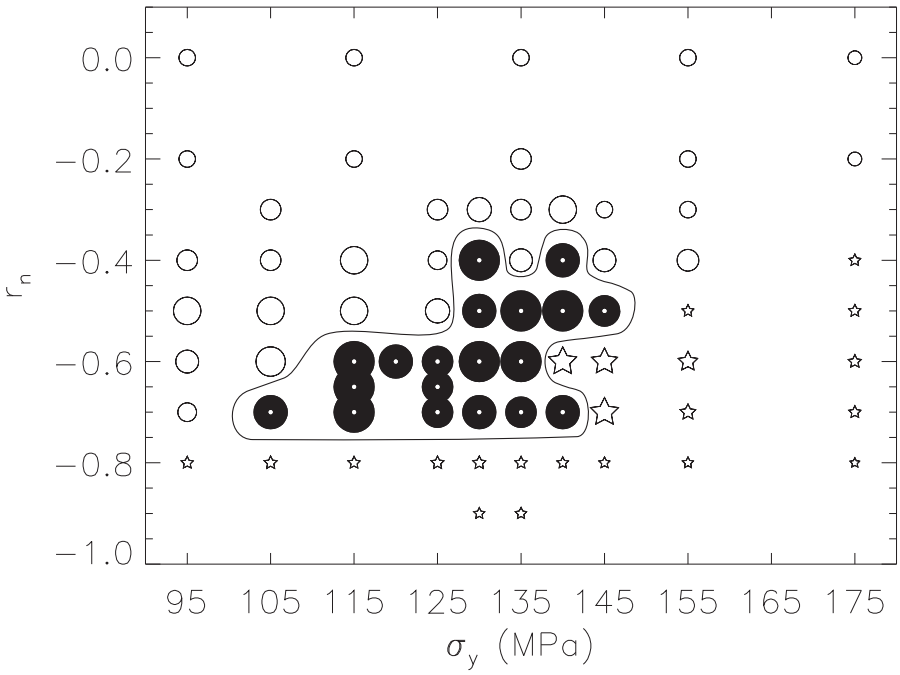

Fig. 10. Type of continental distribution in the σ_y-r_n plot. Little black disks with a white center stand for Earth-like distributions where the size of the disk is a measure of the quality. Five-pointed stars represent an unrealistic multitude of tiny continents. White circles depict runs with reticularly connected, narrow stripe-like continents.

numbers and the volume-averaged temperature as functions of time correspond in the general features with parameterized cooling models. Contrary to the parameterized curves, the curves of [28] show temporal variations. This is more realistic for geological reasons. A well-developed plateness is stable and shows realistic configurations at the surface. The stability of the Earth-like distributed, very thin downwellings is influenced by the pressure dependence of the viscosity connected with the existence of two low-viscosity layers: One layer is the conventional asthenosphere just below the lithosphere. The other one is situated immediately beneath the 660-km phase boundary but the central part of the lower mantle is highly viscous. The latter feature guarantees the relative lateral stability of those plumes which came from the CMB.

Walzer et al. (2006) present an integrated theory, S3, of mantle convection plus chemical differentiation of the growing continental crust and the complementary depleted MORB mantle. Plateness and realistic cooling features of the former step [28] of the model are conserved. The mathematical tools of the

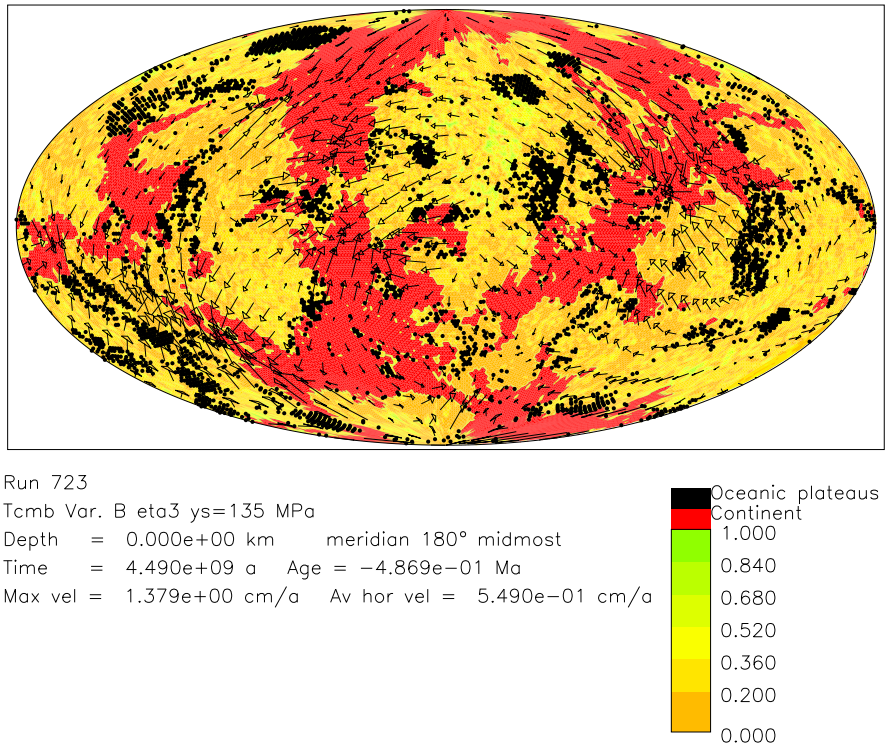

Fig. 11. The distribution of continents (red) and oceanic plateaus (black dots) at the Earth's surface for the geological present of a run with yield stress $\sigma_y = 135$ MPa and a viscosity-level parameter $r_n = -0.5$. Arrows represent creeping velocities.

theory are given in [29]. The complicated geochemical features are discussed there. Some particular items of the chemistry are indicated in Chapter 1 of the present paper.

5 Results and discussions

5.1 Thermal and chemical evolution using a reference run

In this paper, only such numerical results of the new model, S3, are presented that are *not* given in Walzer et al. (2006). To come to the most important item first, the results of this subsection apply also to other runs that are situated in a certain central area of the r_n-σ_y plot. The selected reference run is determined by a yield stress $\sigma_y = 135$ MPa and a viscosity-level parameter $r_n = -0.6$. Now we consecutively present the figures. The corresponding

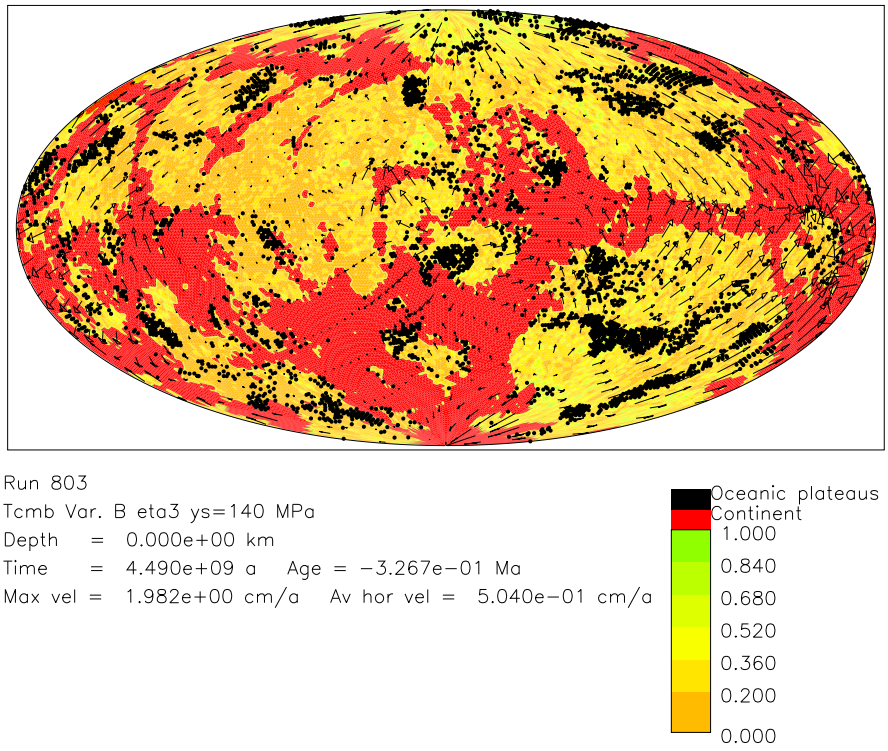

Fig. 12. The distribution of continents (red) and oceanic plateaus (black dots) at the Earth's surface for the geological present of a run with yield stress $\sigma_y = 140$ MPa and a viscosity-level parameter $r_n = -0.5$. Arrows denote creeping velocities.

discussion is immediately after each presentation. In Fig. 1, the laterally averaged temperature is plotted as a function of depth for the geological present time. Its curve is nearer to the parameterized geotherm of whole-mantle convection than to the corresponding temperature curve of layered convection. This is quite understandable since we observe whole-mantle convection in the results of S3. However, the flow is somewhat hindered by the highly viscous transition zone and by the 660-km phase boundary. Therefore the temperature is somewhat elevated but not to such a degree that would be expected for a purely thermal coupling at the 660-km boundary.

Fig. 2 shows the laterally averaged viscosity for the present. The derivation of this type of viscosity profile is given in [26]. We will discuss the profile from below to above: The low viscosity in the D″ layer is determined by the strong temperature gradient at CMB. Therefore the temperature influence on viscosity is larger than the pressure influence in this special zone. The middle part of the lower mantle is highly viscous due to the gradual pressure

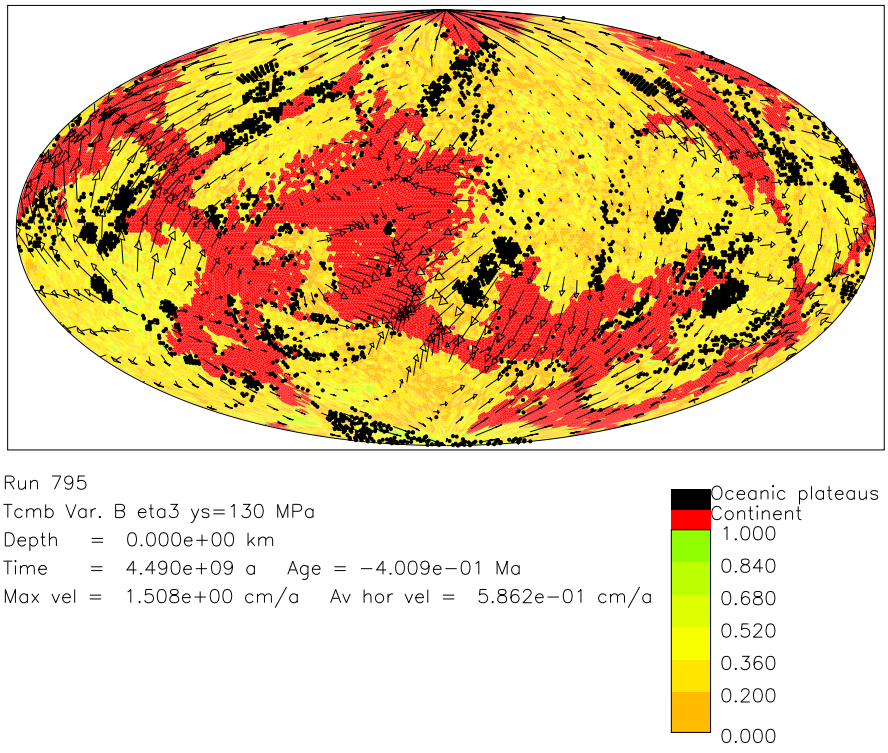

Fig. 13. The distribution of continents (red) and oceanic plateaus (black dots) at the Earth's surface for the geological present of a run with yield stress $\sigma_y = 130$ MPa and a viscosity-level parameter $r_n = -0.4$. Arrows represent creeping velocities.

increase. This causes two effects: *Firstly*, CMB-based plumes use always the same pipe if they have eaten through to the surface. It is energetically more advantageous to use always the same duct instead to burn a new hole in this high-viscosity layer. This is a plausible explanation for the slow lateral movement of the plumes. They move orders of magnitude slower than the lithospheric plates. That's why the plumes can be used as a reference frame for plate motions. Of course, the sluggish lower-mantle bulk convection moves also the tubes of the plume. *Secondly*, chemical inhomogeneity is relatively well conserved in this central part of the lower mantle. It is unimportant for S3 whether this inhomogeneity is primordial or whether it is created by subduction. But if we look for a source region of ^{3}He, ^{20}Ne and ^{22}Ne, than it could be that not only the remains of old and new subduction slabs are conserved in this middle layer of the lower mantle but also parts of a quasi-primordial mantle. The above-said isotopes are not produced in the Earth. On the other hand, it is not very convincing that the mentioned *light* noble

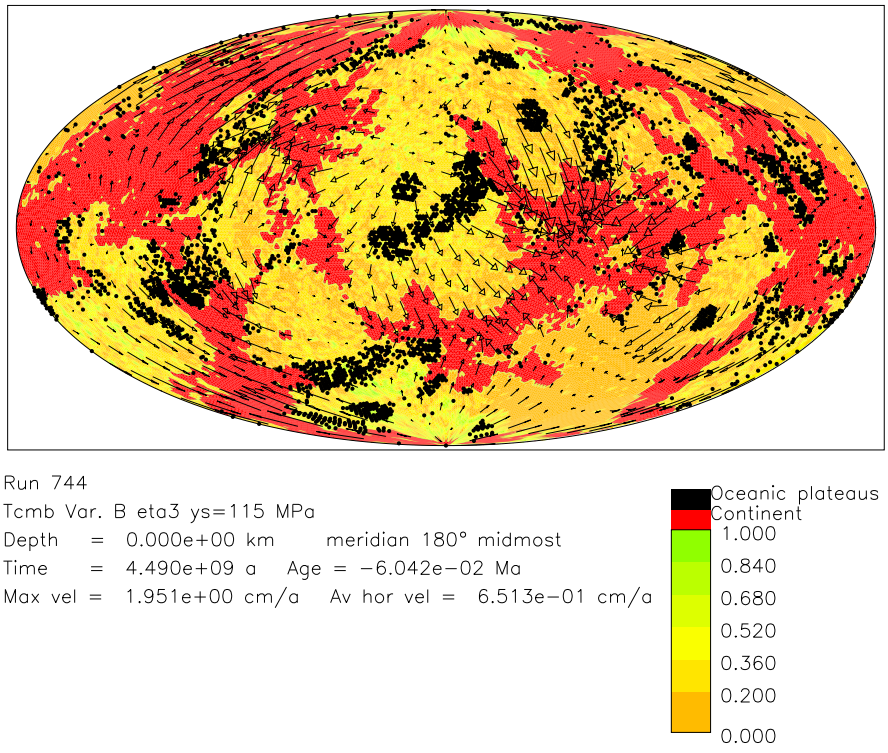

Fig. 14. The distribution of continents (red) and oceanic plateaus (black dots) at the Earth's surface for the geological present of a run with yield stress $\sigma_y = 115$ MPa and a viscosity-level parameter $r_n = -0.7$. Arrows denote creeping velocities.

gases came to the interior by subduction. There are proposals that these nuclides could be primordially stored in the Earth's core. This doesn't seem to be very plausible since the metallic fluid of the outer core moves with 10-30 km/a. So, each part of this iron alloy was very often in contact with the CMB during the Earth's evolution. Therefore we conclude that if the mantle is not able to store the noble gases than the core by no means whatever. However, this discussion is not relevant for the calculations of S3. Fig. 2 indicates a high-viscosity transition zone. It could be that this is true only for a layer between 520 and 660 km depth. The augmentation of the observed seismicity in the transition zone could point to high viscosity. The two low-viscosity layers above and beneath the transition layer cause a strong stirring of the material there. This is a good explanation for the tendency to homogeneity of DMM. Near the surface, Fig. 2 displays a highly viscous lithosphere. Runs with viscosity profiles of other structure show that the two low-viscosity layers

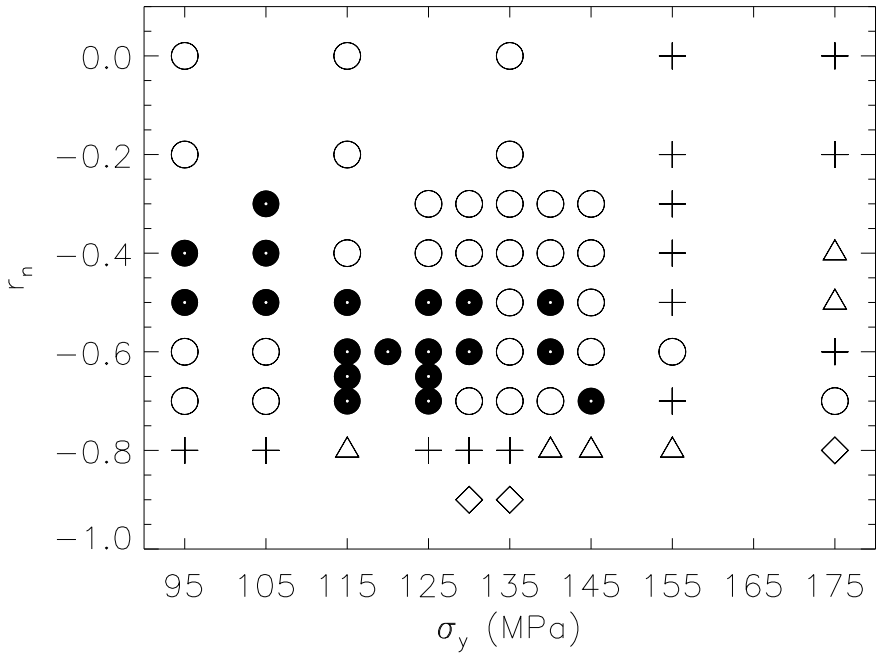

Fig. 15. A classification of the runs using the deviation of the calculated size of present-day continents from the observed size. The quantity d_c is the observed surface percentage of the continents (=40.35%) minus the computed surface percentage of the continents. Little black disks with a white center stand for slight deviations, namely $-4.5 \leq d_c < 4.5$ percent, white circles for $4.5 \leq d_c < 13.5$, plus signs represent $13.5 \leq d_c < 22.5$. White triangles denote runs with $22.5 \leq d_c < 31.5$, white diamonds stand for $31.5 \leq d_c < 40.5$ The quantity d_c of the runs is shown as a function of yield stress, σ_y, and of viscosity-level parameter, r_n.

below the lithosphere and below the 660-km discontinuity are essential for the generation of *very* thin cold sheet-like downwellings.

Fig. 3 represents the temporal dependence of some relevant quantities of the reference run: The first panel exhibits the evolution of laterally averaged heat flow at the Earth's surface. For the present time, the curve arrives at a realistic value: The observed mean global heat flow is 87 mW/m^2 (Pollak et al., 1993). The second panel shows the growth of the total continental mass as a function of time. The behaviour of the model corresponds to the observation that the mantle grew in batches in the geological history (Condie, 2003). The third panel of Fig. 3 displays the temporal dependence of *Ror*. The quantity *Ror* is the reciprocal value of the Urey number. The curve is roughly similar to that of corresponding parameterized models except the smaller variations, of course. The fourth panel of Fig. 3 represents the decrease of the Rayleigh number as a function of time.

Fig. 4 shows similar evolution diagrams: The first panel exhibits the subsiding of the mean temperature. From an age of $\tau = 3000$ Ma, it decreases

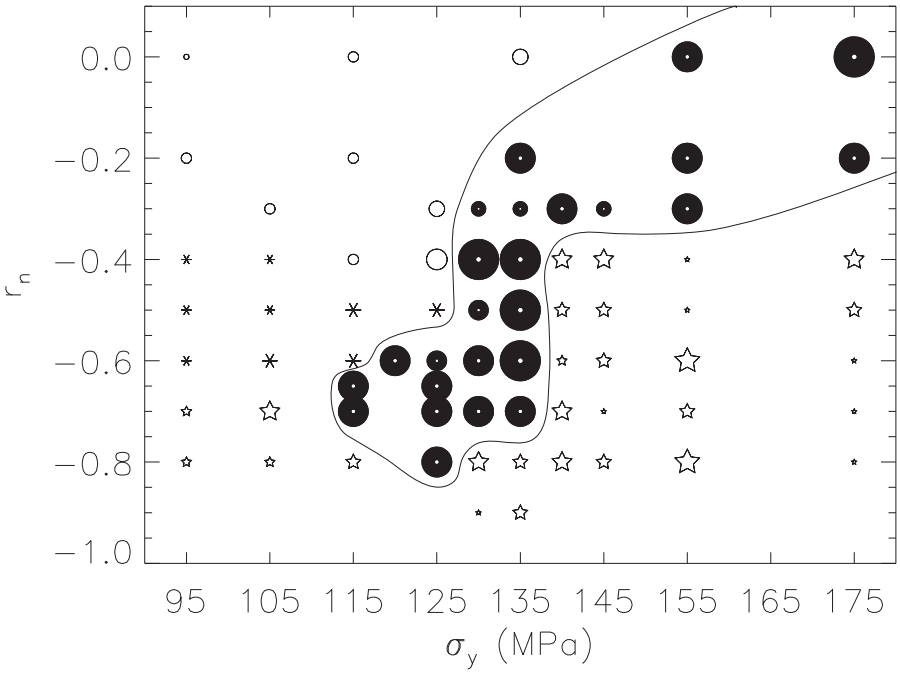

Fig. 16. Plateness in the σ_y-r_n plot. Plate-like solutions with narrow subducting zones are represented by little black disks with a white center. Its surface area is a measure of plateness. White circles stand for runs with broad downwellings and minor plateness. White five-pointed stars denote unrealistic runs with local subduction only. Asterisks represent runs with a rather complex behavior with lots of small, but not narrow downwellings.

until the present time with a gradient of 250 K per 3000 Ma. This is somewhat less than our expectation: From komatiite research we expect 300 K decrease per 3000 Ma. The second panel of Fig. 4 shows the time dependence of the kinetic energy of the upper-mantle flow, *EkinUM*. It is a measure of the power transmission to the laterally moving oceanic lithospheric plates. The third panel of Fig. 4 demonstrates the decrease of the total radiogenic heat production of the mantle.

Fig. 5 displays the distribution of chemical heterogeneity at the end of the chemical evolution of the mantle in a meridional section. There are no pure unblended reservoirs. However, DMM prevails immediately beneath the continents (red) and below the oceanic lithosphere. This is a realistic feature of the model since, where the real lithosphere is ripped, MORB magma flows out if there is no plume in the surrounding. The MORB source (DMM) is depleted and relatively homogenized. This is demonstrated by the low standard deviation of the isotope ratios and of chemical quantities (Allègre and Levin, 1995)

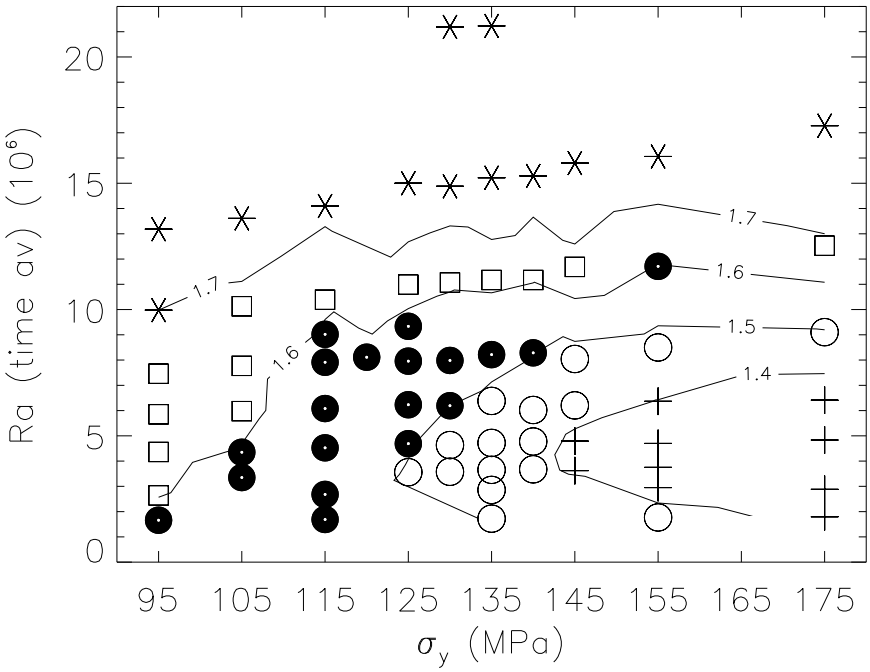

Fig. 17. The time average of the *r*atio of the surface heat *o*utflow per unit time to the mantle's *r*adiogenic heat production per unit time, *Ror*, as a function of the time average of the Rayleigh number, *Ra*, and the yield stress, σ_y. Asterisks denote $1.7 \leq Ror$. White squares stand for $1.6 \leq Ror < 1.7$. Little black disks with a white center represent the realistic range of $1.5 \leq Ror < 1.6$. White circles depict runs with $1.4 \leq Ror < 1.5$. Finally, plus signs stand for $Ror < 1.4$.

although Hofmann (2004) modifies this statement. Fig. 5 shows a marble-cake mantle but reversed than up to now proposed: The *depleted* mantle parts are disconnected and distributed like raisins. It is an important result that we did not obtain simply connected areas for one geochemical reservoir. However, the depleted areas tend to be in the upper parts of the mantle. This is not amazing since they develop below the lithosphere, and the conventional asthenosphere promotes the lateral propagation of DMM because of its low viscosity.

Fig. 6 shows the distribution of continents (red) and of oceanic plateaus (black dots) at the Earth's surface for the geological present time. The moving oceanic lithosphere carries along the oceanic plateaus. If the plateaus touch a continent they will be connected with the continent. This is the only additional implementation. Else, there are no charges or special rules. Neither number nor form nor size of the continents are prescribed. The configuration simply results from the numerical solution of the system of equations and the corresponding initial and boundary conditions. At first, the comparison with the observed continents was done simply visually, then by a development into spherical harmonics using a function of the coefficients, A_n^m and B_n^m, that does not depend on the location of the pole of the coordinate system. We are not

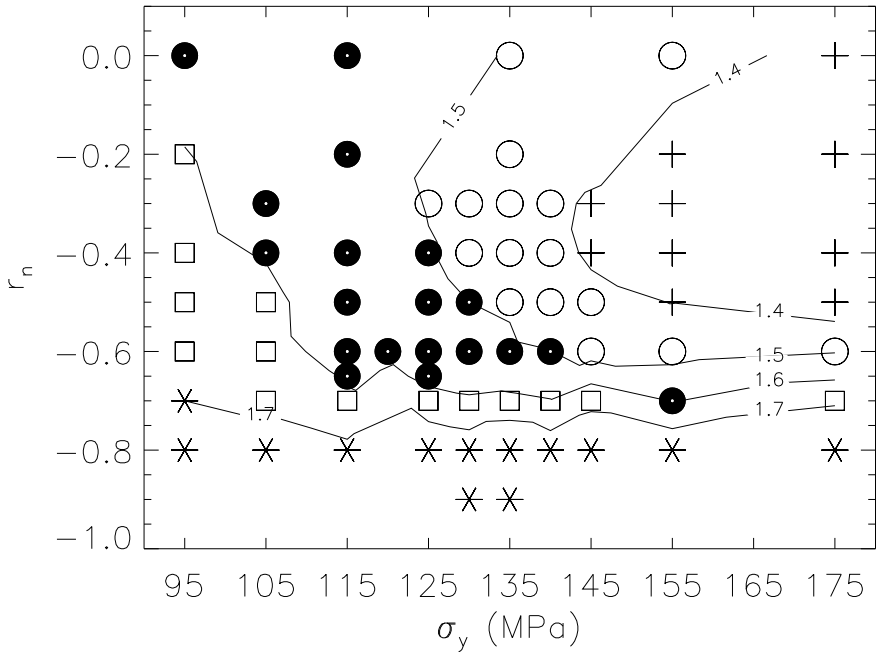

Fig. 18. The magnitude *Ror* as a function of the viscosity-level parameter, r_n, and the yield stress, σ_y. For the description of the symbols, see Fig. 17.

aware of former papers on spherical-shell mantle convection with continents that evolve due to physical laws and which are *not* simply put on the surface.

Fig.7 exhibits a plate-like motion of the lithospheric pieces at the surface. The colors denote the logarithm of the shear viscosity in Pa·s. Fig. 8 displays the present-time temperature on an equal area projection of an interior spherical surface in 134.8 km of depth. The blue lines depict downwelling zones beneath collision lines at surface.

5.2 Variation of parameters: The generation of continents

A multitude of runs were systematically investigated in order to point out that the selected reference run is by no means an exceptional case but it is typical for a certain area of parameters. Furthermore, it is to be demonstrated that the systematic part of the results is not too far from the real Earth. Fig. 9 shows a relatively simple result: The parameter r_n serves for a (single) shift of the starting profile of the viscosity at the beginning of a run. As expected,

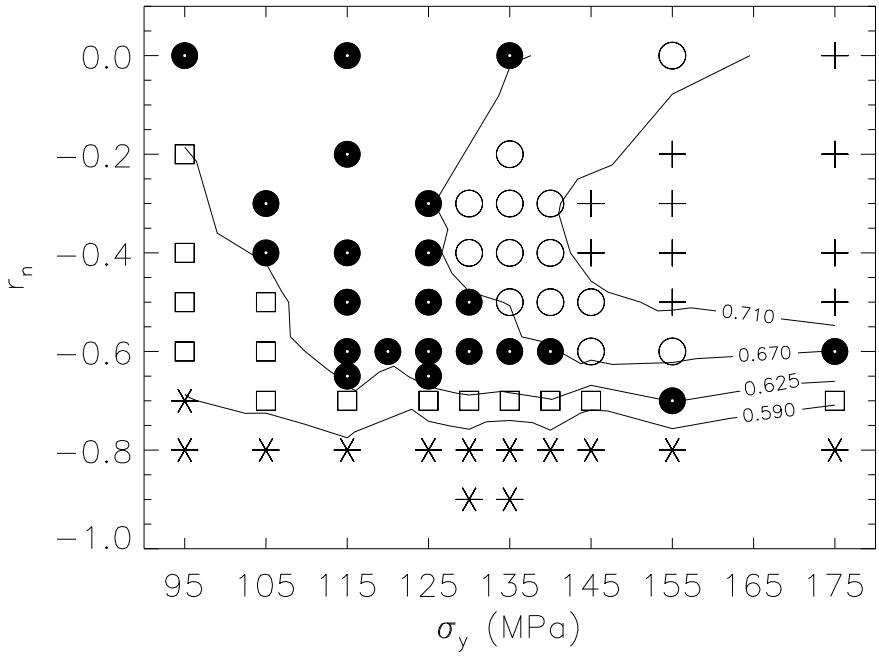

Fig. 19. The time average of the Urey number, Ur, as a function of the viscosity-level parameter, r_n, and the yield stress, σ_y. Asterisks stand for runs with $Ur \leq 0.59$. White squares denote $0.59 < Ur \leq 0.625$. Little black disks with a white center represent runs with $0.625 < Ur \leq 0.67$. White circles signify runs with $0.67 < Ur \leq 0.71$. Plus signs depict runs with $0.71 < Ur$.

Fig. 9 demonstrates that the quantity Ra grows with decreasing r_n because of Eq. (1). There is , however, also a *small* influence of the yield stress.

Size and form of the computed continents have been systematically compared with the observed continents. Fig. 10 exhibits Earth-like continent solutions in the center of an r_n-σ_y plot. These realistic runs are signified by black disks with a white center. A Ra-σ_y plot of the continent quality resembles Fig. 10 since Ra monotonously decreases with increasing r_n. So, the new figure stands on its head. Figs. 11 through 14 show final solutions of the distribution of continents for other input parameters r_n and σ_y, different from those of Fig. 6. Further investigations have been done to restrict the realistic r_n-σ_y area. Fig. 15 displays the distribution of differences, namely observed final continental area minus calculated final continental area. Evidently, a run is only realistic if it has a black disk in Fig. 10 as well as in Fig. 15. But also in this case, a certain middle r_n-σ_y area remains for the favourable solutions.

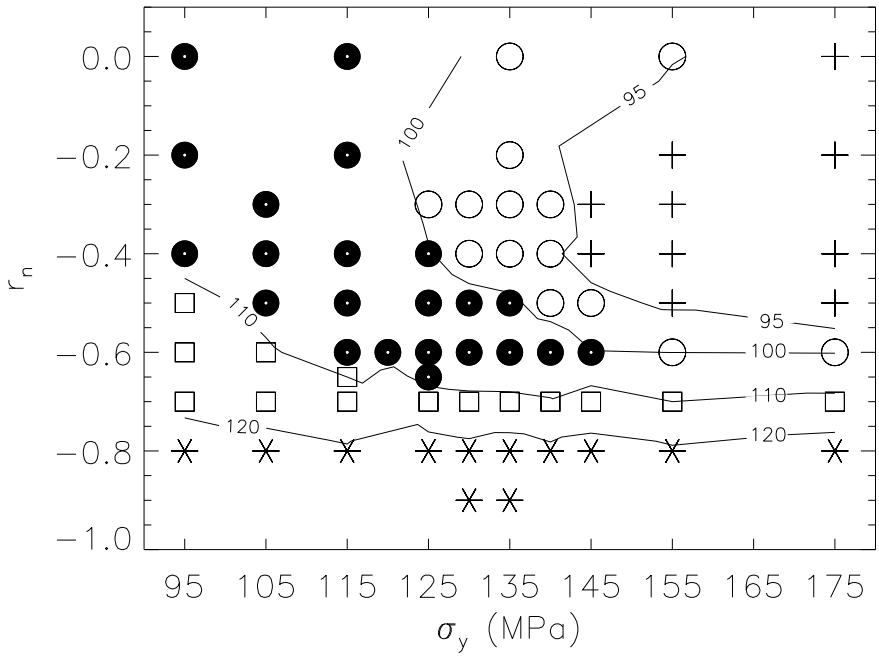

Fig. 20. The symbols represent the classes of the temporal average of the surface average of the heat flow, qob, in a r_n-σ_y plot. The following numbers are given in mW/m^2. Asterisks depict runs with $120 \leq qob$. White squares stand for $110 \leq qob < 120$. Little black disks with a white center denote runs with $100 \leq qob < 110$, white circles are for $95 \leq qob < 100$. Plus signs depics runs with $qob < 95$.

5.3 Variation of the parameters: Generation of plate-like solutions and the distribution of thermal parameters.

Fig. 16 shows a classification of runs regarding the planforms of flows near the surface. Plate-like solutions are represented by black disks. It is indicative of Model S3 that, again, an overlap of the black disks is observed with those of Figs. 10 and 15. Fig. 17 represents the distribution of the time average of the ratio of the heat outflow at the surface to the radiogenic heat generation in the interior, *Ror*, as a function of the time average of the Rayleigh number, *Ra*, and of the yield stress, σ_y. Runs with realistic values of the ratio *Ror* are depicted by black disks. Fig. 18 shows an r_n-σ_y plot of the ratio *Ror*. The Urey number is represented by Fig. 19 in an r_n-σ_y diagram. Finally, the time average of mean surface heat flow for each run are presented in an r_n-σ_y plot. The realistic values are again signified by black disks. We observe a partial covering with the favourable field of continent distribution of Fig. 10. – The conclusions can be found in the Summary.

Acknowledgements

We gratefully acknowledge the supply of computing time by the Höchstleistungsrechenzentrum Stuttgart (HLRS) and by the NIC Jülich.

References

1. Allègre, C.J., and Levin, E. (1995), Isotopic systems and stirring times of the Earth's mantle, *Earth Planet. Sci. Lett.*, *136*, 629-646.
2. Anderson, O.L. (1998), The Grüneisen parameter for iron at outer core conditions and the resulting conductive heat and power in the core, *Phys. Earth Planet. Int.*, *109*, 179-197.
3. Bennett, V.C. (2004), Compositional evolution of the mantle, in *Treatise on Geochemistry*, Vol.2, *The Mantle and the Core*, edited by R.W. Carlson, 493-519, Elsevier, Amsterdam.
4. Bunge, H.-P. (1996), Global mantle convection models, PhD Thesis, University of California, Berkeley.
5. Bunge, H.-P., and Baumgardner, J.R. (1995), Mantle convection modelling on parallel virtual machines, *Computers in physics*, *9*, no. 2, 207-215.
6. Condie, K.C. (2003), Incompatible element ratio in oceanic basalts and komatiites: tracking deep mantle sources and continental growth rates with time, *Geochem. Geophys. Geosyst.*, *4 (1)*, 1005, doi:10.1029/2002GC000333.
7. Dziewonski, A.M., and Anderson, D.L. (1981), Preliminary reference Earth model. *Phys. Earth Planet. Int.*, *25*, 297-356.
8. Fitton, G., Mahoney, J., Wallace, P., and Saunders, A. (eds.) (2004), *Origin and Evolution of the Ontong Java Plateau*, *Geol. Soc. London Spec. Publ.*, *229*.

9. Hofmann, A.W. (2004), Sampling mantle heterogeneity through oceanic basalts: Isotopes and trace elements, in *Treatise an Geochemistry*, Vol. 2, *The Mantle and the Core*, edited by R.W. Carlson, 61-101, Elsevier, Amsterdam
10. Honda, S. and Iwase, Y. (1996), Comparison of the dynamic and parameterized models of mantle convection including core cooling. *Earth Planet. Sci. Lett.*, *139*, 133-145.
11. Kaufmann, G., and Lambeck, K. (2002), Glacial isostatic adjustment and the radial viscosity profile from inverse modeling. *J. Geophys. Res.*, *107*, (B11), 2280,doi:10.1029/2001JB000941.
12. King, S.D., and Masters, G. (1992), An inversion for radial viscosity structure using seismic tomography, Geophys. Res. Lett., *19*, 1551-1554.
13. Norman, M., Borg, L., Nyquist, L. and Bogard, D. (2003), Chonology, geochemistry, and petrology of a ferroan noritic anorthosite clast from Descartes breccia 67215: clues to the age, origin, structure, and impact history of the lunar crust, *Meteorit. Planet. Sci.*, *38*, 645-661.
14. Nyquist, L.E., Bogard, D.D., Shih, C.-Y., Greshake, A., Stoffler, D., and Eugster, O. (2001), Ages and geological histories of martian meteorites, *Space Sci. Rev.*, *96*, 105-164.
15. Pollak, H.N., Hurter, S.J., and Johnson, J.R. (1993), Heat flow from the Earth's interior: analysis of the global data set, *Rev. Geophys.*, *31*, 267-280.
16. Porcelli, D., and Ballentine, C.J. (2002), Models for the distribution of terrestrial noble gases and evolution of the atmosphere, in *Noble Gases in Geochemistry and Cosmochemistry*, edited by D. Porcelli, C.J. Ballentine, and R. Wieler, *Rev. Min. Geochem.*, *47*, 411-480.
17. Rudnick, R.L., and Gao, S. (2004), (eds.) *Treatise on Geochemistry*, Vol. 3, Elsevier, Amsterdam.
18. Schubert, G., Turcotte, D.L., and Olson, P. (2001), *Mantle Convection in the Earth and Planets*, 940 pp., Cambridge Univ. Press, Cambridge, UK.
19. Stacey, F.D., (1992), *Physics of the Earth*, 3rd edn., Brookfield Press, Brisbane, 513 pp.
20. Steinbach, V., Yuen, D.A. and Zhao, W.L. (1993) Instabilities from phase transitions and the timescales of mantle thermal evolution, *Geophys. Res. Lett.*, *20*, 1119-1122.
21. Stevenson, D.J., Spohn, T., and Schubert, G. (1983), Magnetism and thermal evolution of the terrestrial planets. *Icarus*, *54*, 466-489.
22. Stracke, A., Hofmann, A.W., and Hart, S.R. (2005), FOZO, HIMU, and the rest of the mantle zoo, *Gochem. Geophys. Geosyst.*, *6 (5)*, Q05007, doi:10.1029/2004GC000824.
23. Walzer, U., Hendel, R., Baumgardner, J. (2003a), Variation of non-dimensional numbers and a thermal evolution model of the Earth's mantle. In: Krause, E., Jäger, W.(Eds.), High Performance Computing in Science and Engineering '02. Springer-Verlag, Berlin Heidelberg New York. pp. 89-103. ISBN 3-540-43860-2.
24. Walzer, U., Hendel, R., Baumgardner, J. (2003b), Viscosity stratification and a 3D compressible spherical shell model of mantle evolution. In: Krause, E., Jäger, W., Resch, M., (Eds.), High Performance Computing in Science and Engineering '03. Springer-Verlag, Berlin Heidelberg New York. pp. 27-67. ISBN 3-540-40850-9. Model S1

25. Walzer, U., Hendel, R., Baumgardner, J. (2003c), Generation of plate-tectonic behavior and a new viscosity profile of the Earth's mantle. In Wolf,D.,Münster,G.,Kremer,M. (Eds.), NIC Symposium 2004. NIC Series 20, pp. 419-428., ISBN 3-00-012372-5.
26. Walzer, U., Hendel, R., Baumgardner, J. (2004a), The effects of a variation of the radial viscosity profile on mantle evolution. *Tectonophysics*, Volume 384, Issues 1-4, 55-90. Model S2
27. Walzer, U., Hendel, R., Baumgardner, J. (2004b), Toward a thermochemical model of the evolution of the Earth's mantle. In: Krause, E., Jäger, W., Resch, M., (Eds.), High Performance Computing in Science and Engineering '04. Springer-Verlag, Berlin Heidelberg New York. pp 395-454. ISBN 3-540-22943-4.
28. Walzer, U., Hendel, R., Baumgardner, J. (2005), Plateness of the oceanic lithosphere and the thermal evolution of the Earth's mantle. In: Krause, E., Jäger, W., Resch, M., (Eds.), High Performance Computing in Science and Engineering '05. Springer-Verlag, Berlin Heidelberg New York. pp. 289-304. ISBN-10-540-28377-3.
29. Walzer, U., Hendel, R., Baumgardner, J. (2006), An integrated theory of whole-mantle convection, continent generation, and preservation of geochemical heterogenity, *J. Geophys. Res.*, submitted.
30. Yamazaki, D., and Karato, S.-I. (2001), Some mineral physics constraints on the rheology and geothermal structure of the Earth's lower mantle, *American Mineralogist*, *86*, 385-391.
31. Yang, W.-S. (1997), Variable viscosity thermal convection at infinite Prandtl number in a thick spherical shell. *Thesis*, Univ. of Illinois, Urbana-Champaign, 185 pp.